Quantum wave packet and quasiclassical trajectory studies of the reaction H(2S) + CH(X2Π; V = 0, j = 1) → C(1D) + H2(X1 Σ g +): Coriolis coupling effects and stereodynamics

ARTICLE *in* JOURNAL OF COMPUTATIONAL CHEMISTRY · JULY 2013

Impact Factor: 3.59 · DOI: 10.1002/jcc.23309 · Source: PubMed

3 AUTHORS, INCLUDING:

Ruifeng Lu
Nanjing University of Science and Technology
80 PUBLICATIONS **869** CITATIONS
SEE PROFILE

Kaiming Deng
Nanjing University of Science and Technology
98 PUBLICATIONS **738** CITATIONS
SEE PROFILE

Quantum Wave Packet and Quasiclassical Trajectory Studies of the Reaction $H(^2S) + CH(X^2\Pi; v = 0, j = 1) \rightarrow C(^1D) + H_2(X^1\Sigma_g^+)$: Coriolis Coupling Effects and Stereodynamics

Ruifeng Lu,* Yunhui Wang, and Kaiming Deng

The quantum mechanics (QM) and quasiclassical trajectory (QCT) calculations have been carried out for the title reaction with the ground minimal allowed rotational state of CH ($j = 1$) on the 1 $^1A'$ potential energy surface. For the reaction probability at total angular momentum $J = 0$, a similar trend of the QM and QCT calculations is observed, and the QM results are larger than the latter almost in the whole considered energy range (0.1–1.5 eV). The QCT integral cross sections are larger than the QM results with centrifugal sudden approximation, while smaller than those from QM method including Coriolis coupling for collision energies bigger than 0.25 eV. The quantum wave-packet computations show that the Coriolis coupling effects get more and more pronounced with increasing of J. In addition to the scalar properties, the stereodynamical properties, such as the average rotational alignment factor $<P_2(\boldsymbol{j}'\bullet\boldsymbol{k})>$, the angular distributions $P(\theta_r)$, $P(\phi_r)$, $P(\theta_r,\phi_r)$, and the polarization-dependent generalized differential cross sections have been explored in detail by QCT approach. © 2013 Wiley Periodicals, Inc.

DOI: 10.1002/jcc.23309

Introduction

In the past decades, a great deal of attention has been paid to the insertion reaction C + H_2 and its isotopic variants C + HD and C + D_2 because of their importance in atmospheric and combustion chemistry. So far, many experimental studies on this system have been done for understanding the kinetics,[1] the product internal energy distribution[2–6] as well as the dynamic aspects.[4–9]

Being a classical atom-diatom insertion reaction, it also has received plenty of interest in theory. The quantum mechanical (QM) scattering dynamics investigations have been performed, for example, the coupled channel dynamical information including the initial state resolved probabilities, cross sections, and rate coefficients have been obtained by considering two singlet states for the $C(^1D) + H_2(X^1\Sigma_g^+)$ system.[10] The QM and quasiclassical trajectory (QCT) calculations on the second excited 1 $^1A''$ at a collision energy of 80 meV indicated a good agreement between them.[11] The Coriolis interactions, the uncoupled CH_2 states, and permutation inversion symmetry have been taken into account to study the $C(^1D) + H_2$ system dynamics.[12] Subsequently, QM calculations for the isotopic C + HD and C + n-D_2 reactions have been presented, and the importance of the higher singlet state in the dynamics and kinetics of C + n-H_2 was emphasized for the $C(^1D) + H_2$ on the $^1A'$ and $^1A''$ state.[13] The dynamics calculations for the $C(^1D) + H_2$ reaction by the real wave-packet method[10] found that the Renner–Teller effects tend to cut down the probabilites, cross sections, and rate constants compared to the $N(^2D) + H_2$ system[14] in the low energy range by Born–Oppenheimer approximation. Furthermore, the differential and integral cross sections (ICSs) have been calculated by both QM and QCT methods for the reactant rotational quantum states $j = 0$ and 1 of the $C(^1D) + H_2$ reaction.[15] Quantum wave-packet method reported the compuated ICSs, reaction rate constants,[16,17] and the inelastic scattering properties,[18] while the QCT approach have been used to study the translational energy distributions.[19]

With regard to the potential energy surface (PES), the three-dimensional Knowles, Handy, and Carter (KHC) PES has been constructed for the ground triplet state of the CH_2 system, and all the asymptotic regions were accurately described.[20] The ground state PES of methylene has been characterized by multireference configuration interaction calculations and a small barrier for the reaction has been found.[21] An adiabatic global PES of the title system for the lowest singlet state (1 $^1A'$) has been built using the multireference single and double configuration interaction method by Bussery-Honvault, Honvault, and Launay (BHL PES).[22] The BHL PES is depicted schematically in Figure 1a. From this diagram, we know that it is a prototype of an insertion-type barrier-free reaction with a deep well of 4.33 eV for the perpendicular C_{2v} geometry, however, there is a small barrier of 0.54 eV for the linear abstraction mechanism. Recently, a new double many-body expansion (DMBE) PES has been reported by Varandas and coworkers,[23] which has a reaction well of 4.34 eV and a collinear

R. Lu, Y. Wang and K. Deng
Department of Applied Physics, Nanjing University of Science and Technology, Nanjing, 210094, People's Republic of China
E-mail: rflu@njust.edu.cn

Contract grant sponsors: NUST Research Funding; contract grant number: 2011ZDJH05.
Contract grant sponsors: NSF of China; contract grant number: 11004107.

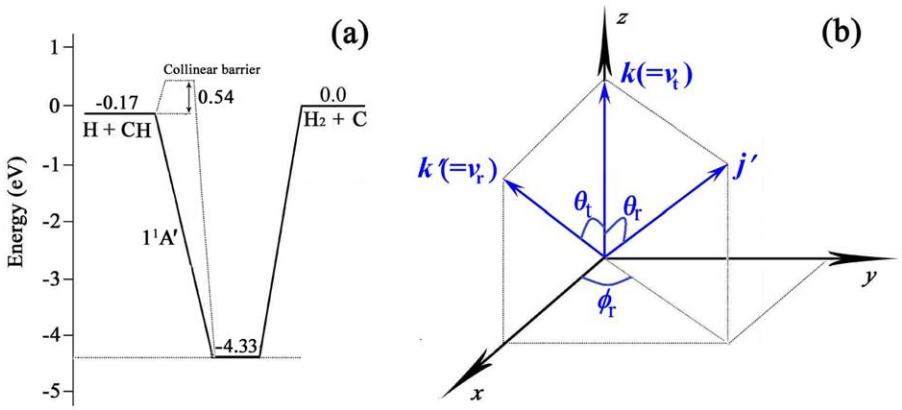

Figure 1. (a) Schematic diagram of the PES for the H (^{2}S) + CH ($X^2\Pi$) → H_2 ($X^1\Sigma^+_g$) + C (^{1}D) reaction. (b)The CM frame used in the description of the vector properties. [Color figure can be viewed in the online issue, which is available at wileyonlinelibrary.com.]

barrier of 0.57 eV, and the energies have been further corrected by the DMBE scaled external correlation method to mimic full configuration interaction.[24–27] The kinetic isotope effect and product branching ratio have been then studied by QCT method based on DMBE PES.[28]

Aforementioned dynamics investigations are related to the forward insertion reaction C + H_2 → H + CH, as for the reverse reaction H + CH → C + H_2, there are some remarkable investigations on the H(^{2}S) + CH($X^2\pi$) → C(^{3}P) + H_2($X^1\Sigma^+_g$) reaction in theory[21,29–32] and experiment.[33–36] However, the reaction H(^{2}S) + CH($X^2\pi$) → C(^{1}D) + H_2($X^1\Sigma^+_g$) has not been studied yet to our knowledge. It should be noted that actually there are nonadiabatic couplings between the four lowest electronic states (^{1}A′, ^{1}A″, ^{3}A″, and ^{3}A′) for the reaction involving the C(^{3}P) atom, such as conical interaction, spin-orbit coupling, and Renner–Teller effect, which could influence the dynamics of the title reaction, especially at high energy region. Although our time-dependent wave-packet (TDWP) method[37,38] and the QM approaches in other works[39–41] on more electronic states succeed in nonadiabatic dynamics studies of various types of reactions, in this article, our motivation is to apply the TDWP and QCT methods to study the title reaction for dynamical scalar properties as well as vector properties (stereo-dynamics) neglecting the nonadiabatic effect, because the adopted BHL 1 ^{1}A′ PES[22] is adiabatic, which corresponds to the H(^{2}S) + CH($X^2\pi$) and C(^{1}D) + H_2($X^1\Sigma^+_g$) asymptotes. However, based on the present work, it is necessary to further explore nonadiabatic feature with the available diabatic PESs. As the lowest allowed rotational state is j =1 for reactant CH($X^2\pi$), in the following calculations, we use its ground vibrational level and the minimal allowed rotational state, and the collision energy is in the range from 0.1 to 1.5 eV.

Computational Details

QM calculations

The QM TDWP method based on second-order split operator coupled to a discrete variable representation with sine basis functions for translational coordinate is standard and referred to the relevant articles[42–44] and the reference therein. The title product pathway from others has been distinguished by analyzing the reaction flux at a fixed surface in the reactant Jacobi coordinates. The following parameters were used to get the converged results of the title reaction: In the reactant Jacobi coordinates, 210 translational basis functions for R grids in the range of 0.1 to 15.0 au at all the collision energy range, 100 vibrational basis functions for r grids in the range of 0.5 to 11.5 au. The total propagation time is 30,000 au, and j_{max} = 80 for rotational basis functions. The calculations with both centrifugal sudden approximation (CS) and close coupling (CC, including the Coriolis coupling) are carried out for comparison, and the projection of J on the body-fixed z-axis, K, is up to 5 in the CC calculations, specifically for the initial projection K_0 is chosen to 0 for both CC and CS calculations.

QCT calculations

The QCT method used in this work is the same with that in literature.[45–49] We use the center-of-mass (CM) frame as shown in Figure 1b, the reagent relative velocity vector ***k*** is parallel to the ***z***-axis, and the ***x-z*** plane is the scattering plane containing the reagent initial vector ***k*** and final product relative velocity vector ***k′***, the ***y***-axis is perpendicular to the ***x-z*** plane. The θ_t is so-called scattering angle that represents the angle between the reagent relative velocity and the product relative velocity. The θ_r and ϕ_r are the polar and azimuthal angles of the final rotational angular momentum ***j′***.

The classical Hamilton equations are integrated numerically for motion in three dimensions in our QCT calculations, and the accuracy of the numerical integration is verified by checking the conservation of the total energy and total angular momentum for every trajectory. We run batches of 100,000 trajectories for each collision energy and the integration step size is 0.1 fs. The trajectories are initiated at a distance of 25.0 Å between the H atom and the CM of the CH diatom. The reaction probability is defined as $P = N_r/N$, which is the ratio of the number of the reactive trajectories N_r to the total number of trajectories N, and for J = 0, it is calculated with the impact parameter b = 0. The ICS, the ***k-j′*** correlation distribution function $P(\theta_r)$, dihedral angular distribution of the ***k-k′-j′***

correlation, and a set of generalized polarization-dependent differential cross section (PDDCSs) are then obtained.

Results and Discussion

Scalar properties

Figure 2 presents the calculated QCT and QM reaction probabilities for total angular momentum $J = 0$ and the total ICSs as a function of collision energy. In Figure 2a, we take notice that the values of the reaction probabilities from both QCT and QM calculations have similar ascending trends with the increasing of collision energy from 0.1 to 0.5 eV. This is ascribed to the property of the 1 ^{1}A′ PES that has a small barrier of 0.54 eV with the linear abstraction pathway. On the contrary, it has a decline trend in the reaction probability when the collision energy changes from 0.6 to 1.5 eV, which is understandable from the deep well of the 1 ^{1}A′ state PES of the H(^{2}S) + CH($X^2\pi$) → C(^{3}P) + H_2($X^1\Sigma_g^+$) reaction. A larger number of resonance peaks in the QM results are originated from the potential well with the complex-forming mechanism. In the whole collision energy range, the QCT reaction probabilities are smaller than the QM results, which is more clear above 0.4 eV, so the tunneling and zero-point energy effects not considered in QCT calculations seems very important in the collision process of H(^{2}S) + CH($X^2\pi$).

In the same collision energy range, we show the ICSs in Figure 2b. The ICS first increases rapidly at low collision energies and then presents a decrease trend with a small fluctuation in a narrow range when the collision energies varied from 0.6 to 0.8 eV. Unlike the QM CS and CC calculations, the QCT results do not indicate any sharp peak structure, it can be understood that the resonances are originated from the quantum effects due to the small barrier and deep well of the PES. There are not so many resonance peak structures obviously in the QM ICS curves because of the *J*-averaging effect washing out the structures. The CC and QCT ICSs are always larger than the corresponding CS ICSs within the whole energy range. In the low energy region, the CC ICSs are smaller than the corresponding QCT ICSs, while above 0.25 eV the CC ICSs are larger than the QCT ones. We note that a small minimum exists at about 0.62 eV of CC calculations, also emerges in the CS ICS, which means the neglect of the coupling between the quantum states of the *J* projection on the body-fixed *z*-axis can still reflect this resonance feature. Nevertheless, the large differences in magnitudes between CS and CC ICSs indicate that the Coriolis coupling should be considered, which is consistent with a recent review devoting to exploring the Coriolis coupling effects in chemical reaction dynamics.[50] Moreover, the obvious discrepances between the QCT and CC results indicate that significant quantum effects affect the title reaction involving two light H atoms.

To address the role of Coriolis coupling in this prototype reaction with the formation of a long-lived complex, as shown in Figures 3a–3f, we present the CS and CC reaction probabilities for H(^{2}S) + CH($X^2\pi$) → C(^{3}P) + H_2($X^1\Sigma_g^+$) with $J = 5$, 10, 20, 30, 40, and 50. Due to the deep well on the 1 ^{1}A′ BHL PES,

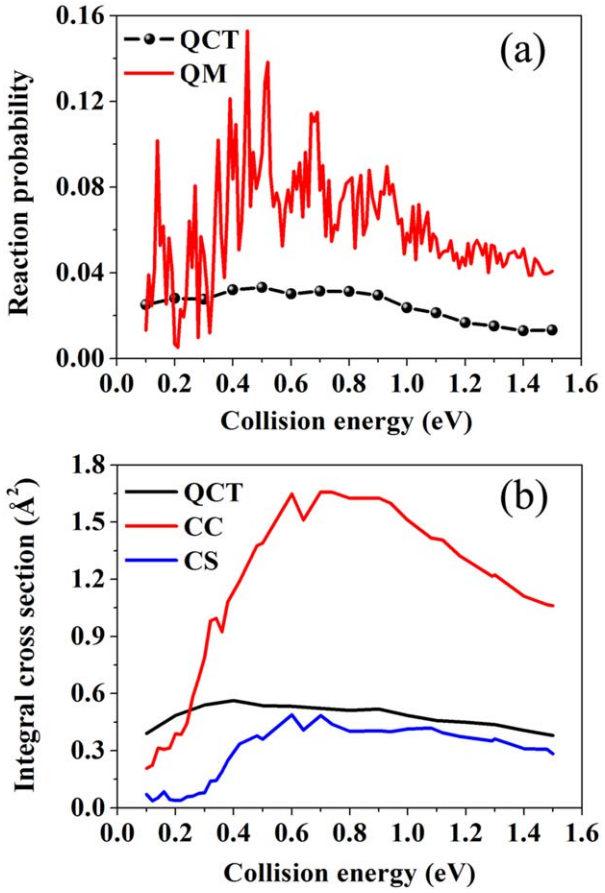

Figure 2. The QCT and QM reaction probabilities ($J = 0$) and ICSs of the H (^{2}S) + CH($X^2\Pi$; $\upsilon = 0$; $j = 0$) → H_2 ($X^1\Sigma^+_g$) + C (^{1}D) reaction as a function of collision energy. [Color figure can be viewed in the online issue, which is available at wileyonlinelibrary.com.]

there are many sharp resonance peaks in the reaction probabilities. Both the CS and CC results display an increasing trend at the beginning, then a decay trend appears with the collision energy increasing. For $J = 5$, the QM CS probabilities are larger than the CC results, while smaller than the CC ones for higher *J*. The CH molecule is confined by just including $K_0 = 0$ quantum states in CS approximation, which increases the opportunity for the sudden collision with H atom and then form the product more easily with fewer resonances for low *J*, leading to overestimation of the reaction probability. As *J* increases to some extent, much more partial waves contribute to the breaking of the collision complex through Coriolis coupling and thus facilitating the formation of the hydrogen molecule. As a result, when the *J* becomes larger, the differences between the CS and CC probabilities are observed to be more and more remarkable, and in more details, the *J*-dependent behavior is observed that the CC probabilities tend to increase with increasing the *J*, as plotted in Figures 3a–3c, then begin to decline as $J = 30$ in Figure 3d. However, such a characteristic is hardly found in CS calculations, which roughly provides a monotonous decreasing trend with *J* increasing. The similar phenomenon can be seen in the dynamics of He + H_2^+.[51] In Figure 3f, the CS values are almost zero as depicted in the inset, and the CC probabilities are almost 60 times larger than the CS ones.

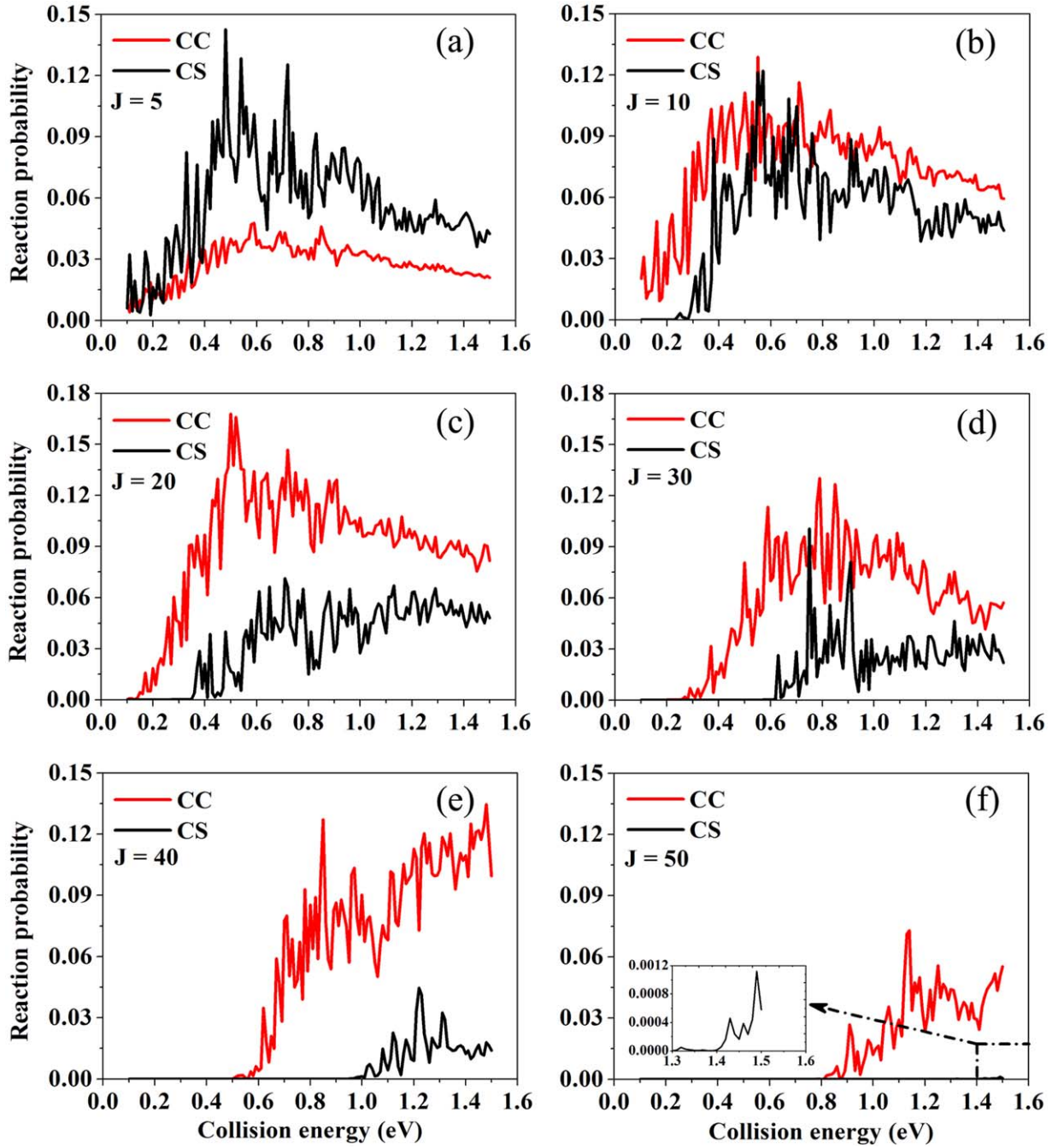

Figure 3. Comparison between the CC and CS probabilities in the collision energy range of 0.1 to 1.5 eV for the total angular momentum (a) $J = 5$; (b) $J = 10$; (c) $J = 20$; (d) $J = 30$; (e) $J = 40$; and (f) $J = 50$. [Color figure can be viewed in the online issue, which is available at wileyonlinelibrary.com.]

The rate coefficients from the two different QM calculations by considering the initial population for singlet state without spin-orbit interaction ($f_{el} = 1/8$)[29,30] are given in Figure 4. From the curves, we can see that the values of the CC calculations are always larger than the corresponding CS rate coefficients. However, both of them have the similar trend that the values decline with the temperature reduced, and the CC rate constant among the range of 10^{-13} to 10^{-11} cm^3/s from 200 to 1000 K indicates the title reaction could be measured in common experiments similar to C + H_2 reaction. The Coriolis coupling effect might be strong different in various reaction system with the complex-forming mechanism or abstraction mechanism, the QM calculations present some general trends with respect to the role in influencing dynamics, although some exceptions are found that CS calculations work well in other complex-forming systems without the long range potential interaction.[52] In the $H(^2S) + CH(X^2\pi, \upsilon = 0, j = 1) \rightarrow C(^3P) + H_2(X^1\Sigma_g^+)$ reaction, it is obvious that the influence of Coriolis coupling on the title reaction is very significant, and neglecting the Coriolis coupling for the title reaction is inappropriate.

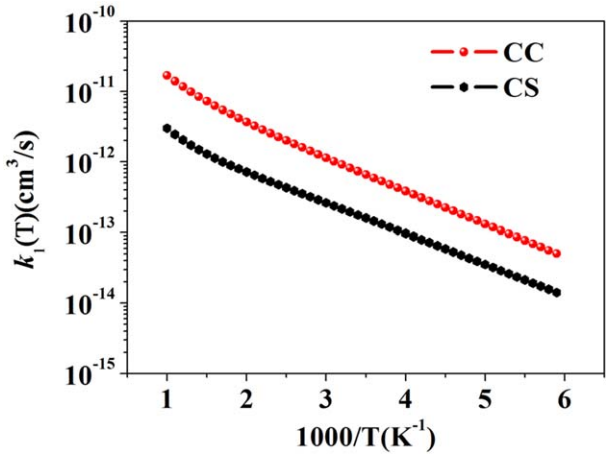

Figure 4. Comparison between the CC and CS rate coefficients of the title reaction. [Color figure can be viewed in the online issue, which is available at wileyonlinelibrary.com.]

Stereodynamics

At present, the measurement of the reagent/product alignment and orientation could be realized with the development of polarized laser techniques. As we know that the values of $<P_2(\boldsymbol{j}'\bullet\boldsymbol{k})>$ could reflect the alignment of products, the dependence of the product rotational alignment on collision energies is plotted in Figure 5. Generally, the higher collision energy causes the stronger rotational alignment of the products. During reactive encounter, the reagent orbital angular momentum completely goes into the product molecule rotational angular momentum, which leads to the product rotational being strongly aligned about the reagents' relative velocity, and the $<P_2(\boldsymbol{j}'\bullet\boldsymbol{k})>$ should be equal to -0.5. We can see that the value of $<P_2(\boldsymbol{j}'\bullet\boldsymbol{k})>$ floats up and down around -0.34 with respect to collision energies, which means that the products have relatively stable and weak alignment. The reason is that the product orbital angular momentum is large and the reactant orbital angular momentum has less influence on the molecular product rotational alignment.

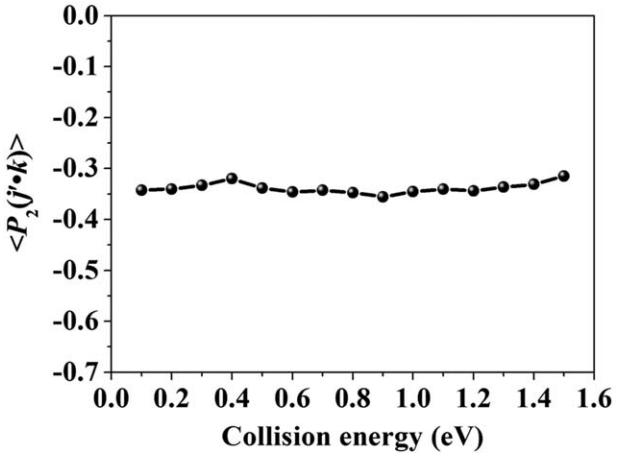

Figure 5. The product rotational alignment of the title reaction as a function of collision energy.

The PDDCSs describe the $\boldsymbol{k}$-$\boldsymbol{k}'$-$\boldsymbol{j}'$ correlation and the scattering direction of the product molecule H_2, which contain rich information about the angular momentum polarization. The calculated PDDCSs for the H + CH → C + H_2 reaction are shown in Figures 6a–6d with the corresponding collision energy changed from 0.1 to 1.5 eV. The PDDCS of $(2\pi/\sigma)(d\sigma_{00}/d\omega_t)$ in Figure 6a is simply proportional to the differential cross section, which describes the $\boldsymbol{k}$-$\boldsymbol{k}'$ correlation or the scattering direction of the products. It is obvious that the products are strongly scattered both forward and backward. The PDDCS of $(2\pi/\sigma)(d\sigma_{20}/d\omega_t)$ in Figure 6b contains the information about the alignment of $\boldsymbol{j}'$ with respect to $\boldsymbol{k}$ as a function of scattering angle. We can see that the behavior of $(2\pi/\sigma)(d\sigma_{20}/d\omega_t)$ shows the opposite trend to that of $(2\pi/\sigma)(d_{00}/d\omega_t)$, which implies that the product rotational angular momentum $\boldsymbol{j}'$ is strongly aligned perpendicular to $\boldsymbol{k}$. In Figures 6c and 6d, the PDDCSs are zero at 0 and π. This is because of that the $\boldsymbol{k}$-$\boldsymbol{k}'$ scattering plane is not determined and the value of PDDCSs with $q \neq 0$ must be zero. When the scattering angles are away from 0 and π, the values of PDDCSs are nonzero, which provides information about the θ_r dihedral angle distribution and indicates the $P(\theta_r,\phi_r)$ distribution is not isotropic for scattering products.

The values of $(2\pi/\sigma)(d\sigma_{22+}/d\omega_t)$ and $(2\pi/\sigma)(d\sigma_{21-}/d\omega_t)$ are related to $<\sin^2\theta_r\cos2\phi_r>$ and $<\sin2\theta_r\cos\phi_r>$, respectively. As it is well known that the negative values of $(2\pi/\sigma)(d\sigma_{22+}/d\omega_t)$ imply the remarkable preference of product alignment along the $\boldsymbol{y}$-axis, by contrary, the positive values indicate the product alignment along the $\boldsymbol{x}$-axis. In Figure 6c, the product alignment is prone to be along the $\boldsymbol{x}$-axis with the increase of the collision energy. As expected at $\theta_t = 30^\circ$, 0.8 eV, the value of $(2\pi/\sigma)(d\sigma_{22+}/d\omega_t)$ is apparently negative, which means the product aligns along the x-axis at this scattering angle. For $(2\pi/\sigma)(d\sigma_{21-}/d\omega_t)$, the positive value indicates the product alignment along the direction of the vector $\boldsymbol{x}$-$\boldsymbol{z}$, and the negative value means the product alignment along the direction of vector $\boldsymbol{x}+\boldsymbol{z}$. While in Figure 6d, the value of $(2\pi/\sigma)(d\sigma_{21-}/d\omega_t)$ is clearly negative at about 15°, indicating the product alignment along the direction of vector $\boldsymbol{x}+\boldsymbol{z}$ with the collision energy varied from 0.1 to 0.3 eV, and it is positive at about 165°, inferring the product alignment along the direction of the vector $\boldsymbol{x}$-$\boldsymbol{z}$ with the collision energy changed from 0.3 to 0.6 eV.

Figure 7 shows the $P(\theta_r)$ distribution for the title reaction, which describes the $\boldsymbol{k}$-$\boldsymbol{j}'$ correlation. Clearly, the $P(\theta_r)$ distribution is symmetric with respect to 90°, and there is a peak at 90° but it is not obvious. According to these findings, we can draw the conclusion that the product rotational angular momentum alignment is perpendicular to the reactant relative velocity, while the polarization is not significant. Overall, there are no clear peak structures with the collision energy increase from 0.1 to 1.5 eV.

The dihedral angle distributions of $P(\phi_r)$, describing the $\boldsymbol{k}$-$\boldsymbol{k}'$-$\boldsymbol{j}'$ correlation, are shown in Figure 8 at collision energies of 0.2, 0.4, 0.6, and 0.8 eV. From the figure we can see that the $P(\phi_r)$ distribution is asymmetric with respect to the $\boldsymbol{k}$-$\boldsymbol{k}'$ scattering plane (or about the $\phi_r = 180^\circ$), which reflects the strong

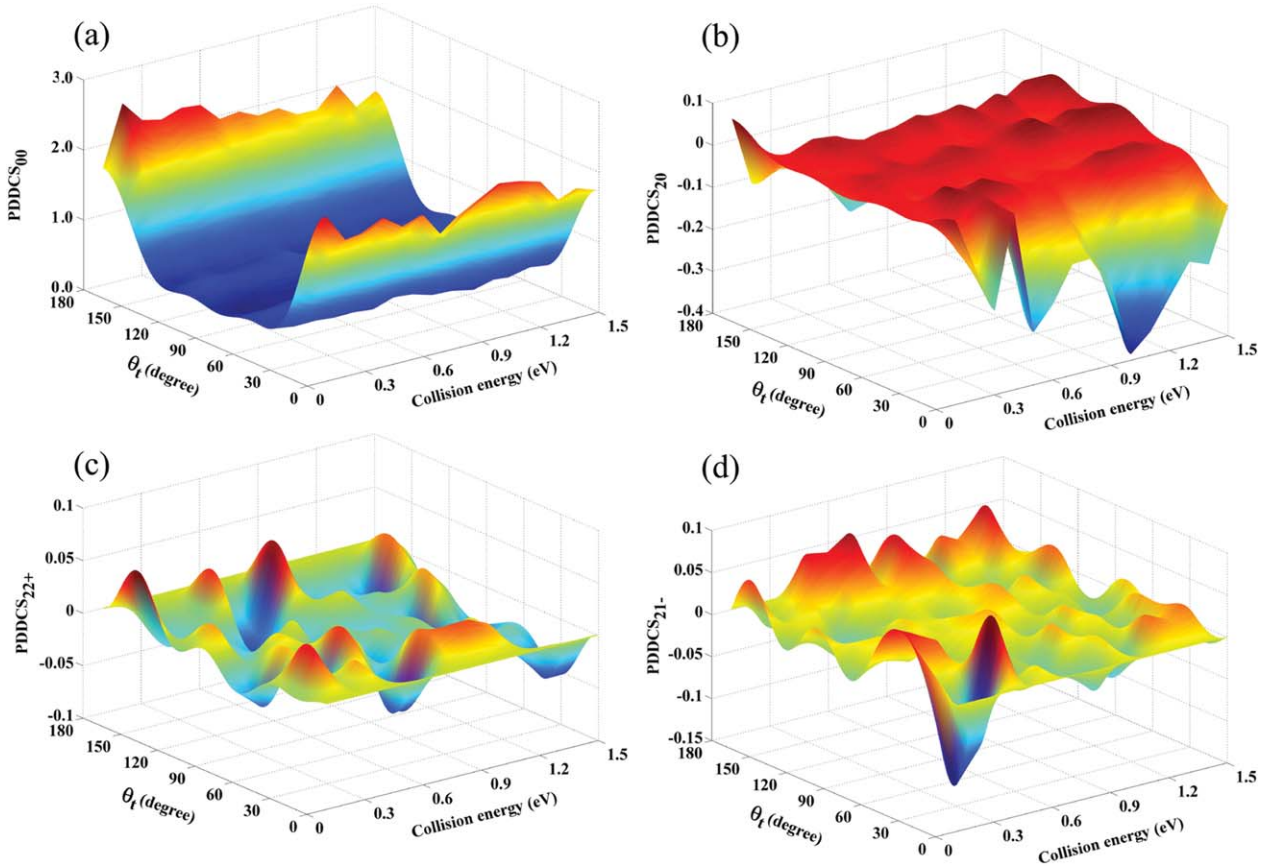

Figure 6. The differential cross sections as functions of both the scattering angle θ_t over the range 0°–180°and the collision energy over the range 0.1–1.5 eV.

polarization of the product rotational angular momentum ***j***′. Furthermore, there is no significant single peak of $P(\phi_r)$ for four different collision energies. That is to say, the preferential ***j***′ orientation of the H_2 molecule along the positive or negative direction of ***y***-axis cannot be observed in the title reaction, which is different from the HOCl system[53] and the C + H_2 reaction.[54]

To check up the tendencies, we plot the angular momentum polarization in the form of polar plots θ_r and ϕ_r averaged over all scattering angles in Figures 9a–9d. As depicted in the figure, the $P(\theta_r,\phi_r)$ distribution is symmetric with respect to θ_r = 90° and is asymmetric with respect to ϕ_r = 180°, which is well consistent with the distribution of $P(\theta_r)$ and $P(\phi_r)$ of the products at collision energies of 0.2, 0.4, 0.6, and 0.8 eV. The distributions $P(\theta_r,\phi_r)$ indicate that the products are weakly polarized perpendicular to the scattering plane and do not mainly rotate in planes parallel to the scattering plane.

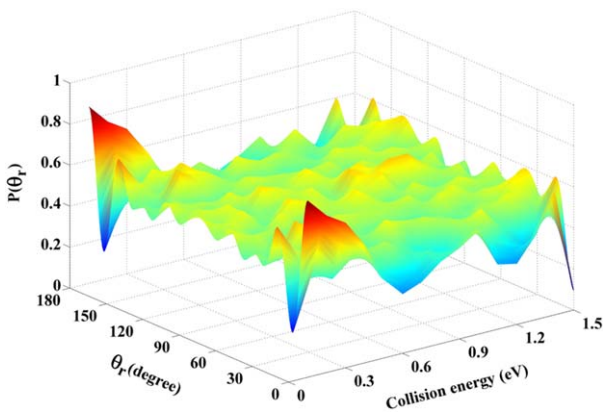

Figure 7. The angular distribution of $P(\theta_r)$ reflecting ***k***-***j***′ correlation as functions of both the angle θ_r over the range 0°–180° and the collision energy over the range 0.1–1.5 eV. [Color figure can be viewed in the online issue, which is available at wileyonlinelibrary.com.]

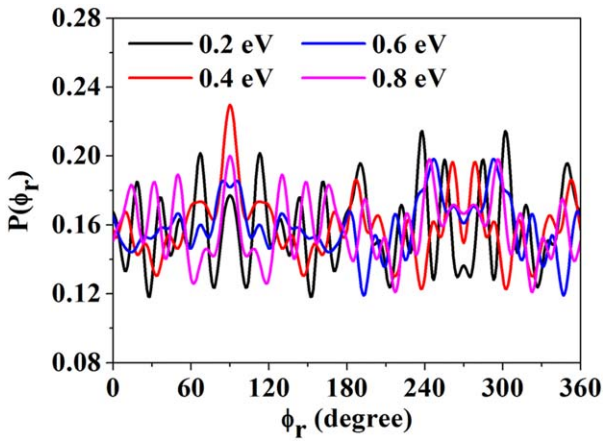

Figure 8. The angular distribution of $P(\phi_r)$ as a function of the dihedral angle ϕ_r at four collision energies of 0.2, 0.4, 0.6, and 0.8 eV. [Color figure can be viewed in the online issue, which is available at wileyonlinelibrary.com.]

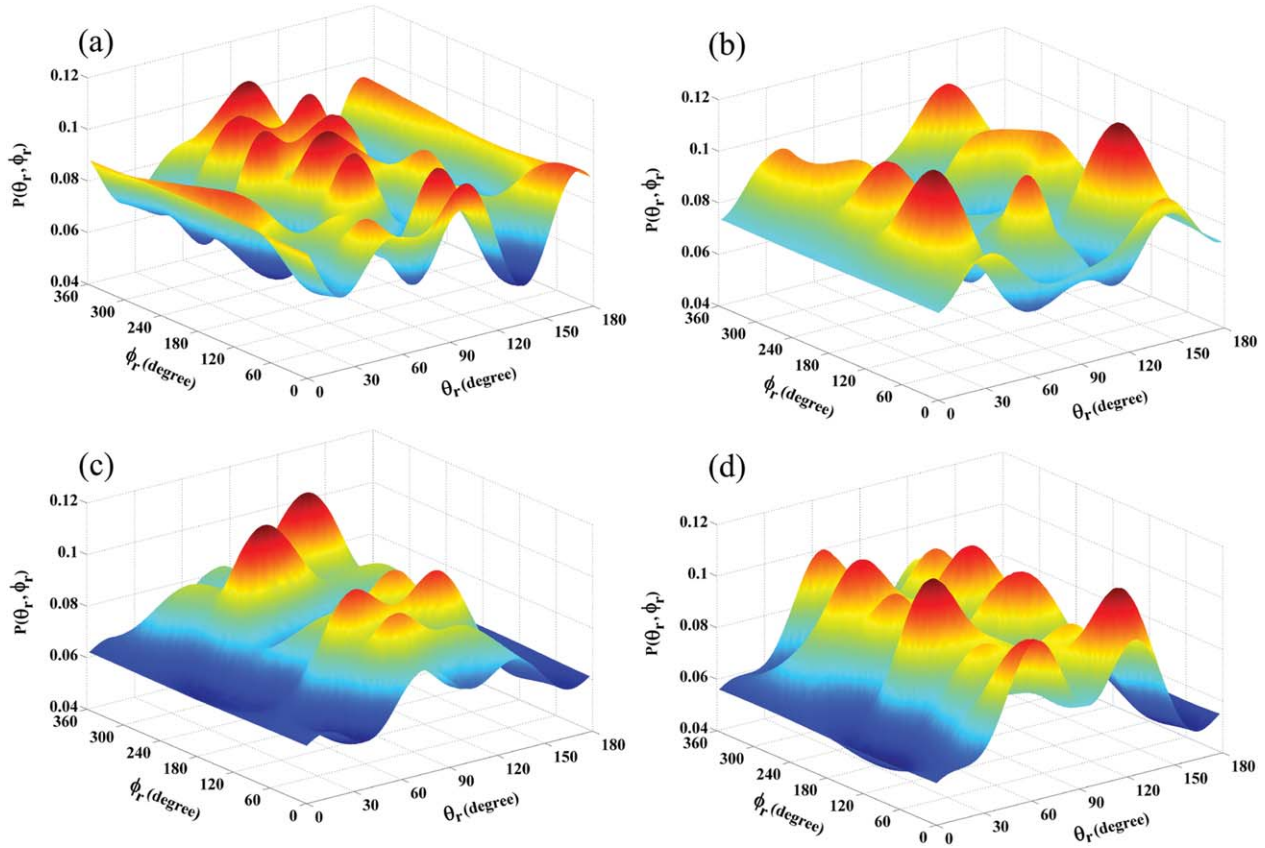

Figure 9. The angular momentum polarization distribution of $P(\theta_r, \phi_r)$ at (a) 0.2 eV, (b) 0.4 eV, (c) 0.6 eV, and (d) 0.8 eV as functions of both θ_r in the range of 0°–180° and ϕ_r in the range of 0°–360°.

Conclusions

In summary, we have performed QM and QCT calculations for the reaction of H + CH ($\upsilon = 0; j = 1$) → H_2 + C on the lowest singlet state PES. The reaction probability and ICS are predicted to increase at the beginning, and then decrease along with the increase of collision energy. The QM reaction probabilities at total angular momentum $J = 0$ is larger than that by QCT method, indicating that quantum effects should be included. Also, the ICSs and rate coefficients of the CC calculations are always larger than the corresponding CS results. The comparison between the CS and CC calculations reveals that the Coriolis coupling is very important for accurate dynamics calculations of this reaction. In addition, we have investigated the vector properties of the product by QCT approach. The values of $<P_2(\boldsymbol{j}'\cdot\boldsymbol{k})>$ with respect to collision energies, indicating that the rotational alignments of the products are stable and relatively weak. The calculated normalized PDDCSs show that the products are both strongly scattered forward and backward. We also attained the distribution curves of $P(\theta_r)$, $P(\phi_r)$, and $P(\theta_r,\phi_r)$ of the title reaction. The product rotational angular momentum $\boldsymbol{j}'$ appears to have no preferential orientation along the $\boldsymbol{y}$-axis, and the $\boldsymbol{j}'$ is perpendicular to the reactant relative velocity, while the polarization is not significant. Please keep in mind that there are other effects affecting the dynamics of all channels (additional nonreactive H + CH → H + CH and H exchange reaction H + CH′ → H′ + CH), such as the nonadiabatic coupling through other electronic states, we will pursue further investigations when the appropriate potential surfaces are available.

Acknowledgments

The authors sincerely thank Prof. Keli Han for providing us the computational code.

Keywords: time-dependent quantum wave-packet · quasiclassical trajectory · Coriolis coupling · centrifugal sudden · stereodynamics

How to cite this article: R. Lu, Y. Wang, K. Deng, *J. Comput. Chem.* **2013**, *34*, 1735–1742. DOI: 10.1002/jcc.23309

[1] D. Husain, P. E. Norris, *Faraday Discuss. Chem. Soc.* **1979**, *67*, 273.
[2] G. M. Jursich, J. R. Wiesenfeld, *Chem. Phys. Lett.* **1984**, *110*, 14.
[3] G. M. Jursich, J. R. Wiesenfeld, *J. Chem. Phys.* **1985**, *83*, 910.
[4] W. H. Fisher, T. Carrington, C. M. Sadowski, C. H. Dugan, *Chem. Phys.* **1985**, *97*, 433.
[5] D. C. Scott, J. De Juan, D. C. Robie, D. Schwartz-Lavi, H. Reisler, *J. Phys. Chem.* **1992**, *96*, 2509.
[6] K. Mikulecky, K.-H. Gericke, *J. Chem. Phys.* **1993**, *98*, 1244.
[7] M. R. Scholefield, S. Goyal, J.-H. Choi, H. J. Reisler, *J. Phys. Chem.* **1995**, *99*, 14605.
[8] K. Sato, N. Ishida, T. Kurakata, A. Iwasaki, S. Tsuneyuki, *Chem. Phys. Lett.* **1998**, *237*, 195.

[9] A. Bergeat, L. Cartechini, N. Balucani, G. Capozza, L. F. Philips, P. Casavecchia, G. G. Volpi, L. Bonnet, J.-C. Rayez, *Chem. Phys. Lett.* **2000**, *327*, 197.
[10] P. Defazio, B. Bussery-Honvault, P. Honvault, C. Petrongolo, *J. Chem. Phys.* **2011**, *135*, 114308.
[11] P. Honvault, B. Bussery-Honvault, J. -M. Launay, F. J. Aoiz, L. Bañares, *J. Chem. Phys.* **2006**, *124*, 154314.
[12] P. Defazio, C. Petrongolo, B. Bussery-Honvault, P. Honvault, *J. Chem. Phys.* **2009**, *131*, 114303.
[13] P. Defazio, P. Gamallo, M. González, S. Akpinar, B. Bussery-Honvault, P. Honvault, C. Petrongolo, *J. Chem. Phys.* **2010**, *132*, 104306.
[14] P. Gamallo, P. Defazio, M. González, C. Petrongolo, *J. Chem. Phys.* **2008**, *129*, 244307.
[15] L. Bañares, F. J. Aoiz, P. Honvault, B. Bussery-Honvault, J. M. Launay, *J. Chem. Phys.* **2003**, *118*, 565.
[16] F. Gogtas, N. Bulut, S. Akpinar, *Int. J. Quantum. Chem.* **2005**, *105*, 478.
[17] S. Y. Lin, H. Guo, *J. Phys. Chem. A* **2004**, *108*, 2141.
[18] S. Y. Lin, H. Guo, *J. Chem. Phys.* **2003**, *119*, 11602.
[19] N. Balucani, G. Capozza, L. Cartechini, A. Bergeat, R. Bobbenkamp, P. Casavecchia, F. J. Aoiz, L. Bañares, P. Honvault, B. Bussery-Honvault, J. M. Launay, *Phys. Chem. Chem. Phys.* **2004**, *6*, 4957.
[20] P. Knowles, N. C. Handy, S. Carter, *Mol. Phys.* **1983**, *49*, 681.
[21] L. B. Harding, R. Guadagnini, G. C. Schatz, *J. Phys. Chem.* **1993**, *97*, 5472.
[22] B. Bussery-Honvault, P. Honvault, J. M. Launay, *J. Chem. Phys.* **2001**, *115*, 10701.
[23] S. Joseph, A. J. C. Varandas, *J. Phys. Chem. A* **2009**, *113*, 4175.
[24] A. J. C. Varandas, *J. Mol. Struct. Theochem.* **1985**, *120*, 401.
[25] A. J. C. Varandas, *Adv. Chem. Phys.* **1988**, *74*, 255.
[26] A. J. C. Varandas, *Chem. Phys. Lett.* **1992**, *194*, 333.
[27] A. J. C. Varandas, A. I. Voronin, *Mol. Phys.* **1995**, *85*, 497.
[28] S. Joseph, P. J. S. B. Caridade, A. J. C. Varandas, *J. Phys. Chem. A* **2011**, *115*, 7882.
[29] P. Gamallo, P. Defazio, S. Akpinar, C. Petrongolo, *J. Phys. Chem. A* **2012**, *116*, 8291.
[30] R. van Harrevelt, M. C. van Hemert, G. C. Schatz, *J. Chem. Phys.* **2002**, *116*, 6002.
[31] P. Jensen, P. R. Bunker, *J. Chem. Phys.* **1988**, *89*, 1327.
[32] J. N. Murrel, L. J. Dunne, *J. Chem. Phys. Lett.* **1983**, 102, 155.
[33] K. H. Becker, B. Engelhardt, P. Wiesen, K. D. Bayes, *Chem. Phys. Lett.* **1989**, *154*, 342.
[34] A. J. Dean, D. F. Davidson, R. K. Hanson, *J. Phys. Chem.* **1991**, *95*, 183.
[35] A. J. Dean, R. F. Hanson, *Int. J. Chem. Kinet.* **1992**, *24*, 517.
[36] J. Peeters, C. Vinckier, 15th Symposium (International) on Combustion, The Combustion Institute, Pittsburgh, **1975**, p. 969.
[37] T. X. Xie, Y. Zhang, M. Y. Zhao, K. L. Han, *Phys. Chem. Chem. Phys.* **2003**, *5*, 2034.
[38] T. S. Chu, Y. Zhang, K. L. Han, *Int. Rev. Phys. Chem.* **2006**, *25*, 201.
[39] K. Drukker, G. C. Schatz, *J. Chem. Phys.* **1999**, *111*, 2451.
[40] T. Takayanagi, *J. Chem. Phys.* **2002**, *116*, 2439.
[41] M. H. Alexander, D. E. Manolopoulos, H. J. Werner, *J. Chem. Phys.* **2000**, *113*, 11084.
[42] D. H. Zhang, J. Z. H. Zhang, *J. Chem. Phys.* **1993**, *99*, 5615.
[43] R. F. Lu, P. Y. Zhang, T. S. Chu, T. X. Xie, K. L. Han, *J. Chem. Phys.* **2007**, *126*, 124304.
[44] T. S. Chu, K. L. Han, *J. Phys. Chem. A*, **2005**, *109*, 2050.
[45] K. L. Han, G. Z. He, N. Q. Lou, *J. Chem. Phys.* **1996**, *105*, 8699.
[46] R. J. Li, K. L. Han, F. E. Li, R. C. Lu, G. Z. He, N. Q. Lou, *Chem. Phys. Lett.* **1994**, *220*, 281.
[47] M. L. Wang, K. L. Han, G. Z. He, *J. Phys. Chem. A* **1998**, *102*, 10204.
[48] M. L. Wang, K. L. Han, G. Z. He, *J. Chem. Phys.* **1998**, *109*, 5446.
[49] Y. H. Guo, F. Y. Zhang, H. Z. Ma, *Commun. Comput. Chem.* **2013**, *1*, 99.
[50] E. L. Wu, *J. Comput. Chem.* **2010**, *31*, 2827.
[51] T. S. Chu, R. F. Lu, K. L. Han, *J. Chem. Phys.* **2005**, *122*, 244322.
[52] T. S. Chu, K. L. Han, *Phys. Chem. Chem. Phys.* **2008**, *10*, 2431.
[53] S. W. Zhou, Y. H. Wang, R. F. Lu, *Chem. Phys.* **2012**, *402*, 113.
[54] L. H. Kang, *Int. J. Quantum. Chem.* **2011**, *111*, 117.

Received: 26 December 2012
Revised: 1 April 2013
Accepted: 9 April 2013
Published online on 14 May 2013